Biomaterials 73 (2015) 12–22

Contents lists available at ScienceDirect

Biomaterials

journal homepage: www.elsevier.com/locate/biomaterials

Multimodality noninvasive imaging for assessing therapeutic effects of exogenously transplanted cell aggregates capable of angiogenesis on acute myocardial infarction

Chieh-Cheng Huang [a, 1], Hao-Ji Wei [b, c, 1], Kun-Ju Lin [d, e], Wei-Wen Lin [f, g], Ching-Wen Wang [a], Wen-Yu Pan [a, b], Shiaw-Min Hwang [h], Yen Chang [b, **], Hsing-Wen Sung [a, *]

[a] Department of Chemical Engineering and Institute of Biomedical Engineering, National Tsing Hua University, Hsinchu, Taiwan, ROC
[b] Division of Cardiovascular Surgery, Veterans General Hospital–Taichung, and College of Medicine, National Yang-Ming University, Taipei, Taiwan, ROC
[c] Division of Cardiovascular Surgery, Chiayi Branch, Veterans General Hospital–Taichung, Chiayi, Taiwan, ROC
[d] Healthy Aging Research Center, Department of Medical Imaging and Radiological Sciences, College of Medicine, Chang Gung University, Taoyuan, Taiwan, ROC
[e] Department of Nuclear Medicine and Center of Advanced Molecular Imaging and Translation, Chang Gung Memorial Hospital, Linkou, Taiwan, ROC
[f] Division of Cardiology, Veterans General Hospital–Taichung, Taichung, Taiwan, ROC
[g] Department of Life Science, Tunghai University, Taichung, Taiwan, ROC
[h] Bioresource Collection and Research Center, Food Industry Research and Development Institute, Hsinchu, Taiwan, ROC

ARTICLE INFO

Article history:
Received 1 June 2015
Received in revised form
1 September 2015
Accepted 9 September 2015
Available online 11 September 2015

Keywords:
Cellular cardiomyoplasty
Vasculogenesis
Cell-based therapy
Ischemic diseases
Translational medicine

ABSTRACT

Although the induction of neovascularization by cell-based approaches has demonstrated substantial potential in treating myocardial infarction (MI), the process of cell-mediated angiogenesis and its correlation with therapeutic mechanisms of cardiac repair remain elusive. In this work, three-dimensional (3D) aggregates of human umbilical vein endothelial cells (HUVECs) and cord-blood mesenchymal stem cells (cbMSCs) are constructed using a methylcellulose hydrogel system. By maximizing cell–cell and cell–ECM communications and establishing a hypoxic microenvironment in their inner cores, these cell aggregates are capable of forming widespread tubular networks together with the angiogenic marker $\alpha_v\beta_3$ integrin; they secret multiple pro-angiogenic, pro-survival, and mobilizing factors when grown on Matrigel. The aggregates of HUVECs/cbMSCs are exogenously engrafted into the peri-infarct zones of rats with MI *via* direct local injection. Multimodality noninvasive imaging techniques, including positron emission tomography, single photon emission computed tomography, and echocardiography, are employed to monitor serially the beneficial effects of cell therapy on angiogenesis, blood perfusion, and global/regional ventricular function, respectively. The myocardial perfusion is correlated with ventricular contractility, demonstrating that the recovery of blood perfusion helps to restore regional cardiac function, leading to the improvement in global ventricular performance. These experimental data reveal the efficacy of the exogenous transplantation of 3D cell aggregates after MI and elucidate the mechanism of cell-mediated therapeutic angiogenesis for cardiac repair.

1. Introduction

The induction of therapeutic angiogenesis by cell-based transplantation has been shown to have substantial potential for treating limb or myocardial ischemia [1,2]. Before transplantation, cells of the desired types must be grown on a large scale *in vitro* and then dissociated from their culture dishes using proteolytic enzymes. The retention of intramuscularly injected dissociated cells at engrafted sites is reportedly problematic [3]. The poor cell retention

* Corresponding author. Department of Chemical Engineering, National Tsing Hua University, Hsinchu 30013, Taiwan, ROC.
** Corresponding author.
E-mail addresses: ychang@vghtc.gov.tw (Y. Chang), hwsung@mx.nthu.edu.tw (H.-W. Sung).
[1] The first two authors (C.C. Huang and H.J. Wei) contributed equally to this work.

http://dx.doi.org/10.1016/j.biomaterials.2015.09.009
0142-9612/

adversely influences the efficacy of cell-transplantation therapy, suggesting that the cell delivery strategy warrants further refinement [4].

To promote the success of cell engraftment for therapeutic angiogenesis, our group has developed a cell delivery strategy that involves three-dimensional (3D) cell aggregates that are assembled in a thermo-responsive methylcellulose (MC) hydrogel system [5–8]. The cell aggregates that are capable of angiogenesis consisted of human umbilical vein endothelial cells (HUVECs) and cord-blood mesenchymal stem cells (cbMSCs). To ensure vascular maturation and stability, ECs must functionally interact with mural cells such as pericytes or smooth muscle cells (SMCs) [9]. Investigations have shown that MSCs can differentiate into pericytes and SMCs [10]. Assembling cells into 3D aggregates enables the cell–cell and cell–extracellular matrix (ECM) interactions to be re-established, forming a native tissue-mimicking microenvironment [11,12]. Using a mouse model of hindlimb ischemia, the 3D cell aggregates that were transplanted intramuscularly *via* local injection were demonstrated to be entrapped effectively in the interstices of muscular tissues and then to adhere to engraftment sites [7,13]. The engrafted cells subsequently promoted considerable angiogenesis, improving the regional perfusion and salvaging the ischemic limb.

Although the therapeutic efficacy of HUVEC/cbMSC aggregates appears to be favorable, the mechanism of their angiogenesis in repairing ischemic tissues remains elusive. As one of the key cell-surface receptors and adhesion molecules in initiating and regulating angiogenesis, $\alpha_v\beta_3$ integrin is strongly expressed by ECs during neovascular growth [14,15]. The expression of integrins modulates the migration of angiogenic vessels by enabling ECs to adhere to ECM [16]. Furthermore, $\alpha_v\beta_3$ integrin associates with growth-factor receptors, facilitating their activation for angiogenesis [16,17]. The important roles of $\alpha_v\beta_3$ integrin in angiogenesis make it a potential target for the noninvasive imaging of angiogenesis [14].

This study extends our earlier observations by elucidating the process of cell-mediated angiogenesis and its therapeutic effects that are induced by exogenously engrafted HUVEC/cbMSC aggregates in rats with myocardial infarction (MI), using multimodality noninvasive imaging methods. Noninvasive methods for the evaluation of angiogenesis, myocardial perfusion, and cardiac function would be valuable in reducing the number of animals required and limiting inter-subject variability, as each animal could be imaged repeatedly.

To elucidate the beneficial effects of cell aggregates in treating MI, $\alpha_v\beta_3$ integrin was used as an imaging target to track the angiogenic process after cell treatment by positron emission tomography (PET). Blood perfusion recovery, global cardiac function, and regional myocardial strains were evaluated using single photon emission computed tomography (SPECT) and echocardiography, respectively. PET and SPECT are noninvasive molecular imaging modalities for assessing responses to cell therapies that involve the stimulation of angiogenesis. Measurements of myocardial 2D strains by a noninvasive echocardiographic technique offer a sensitive means of detecting changes in regional contraction during ischemia.

2. Materials and methods

2.1. Cell culture

Human cbMSCs and HUVECs were obtained from Bioresource Collection and Research Center, Food Industry Research and Development Institute, Hsinchu, Taiwan. The cbMSCs, which were transfected non-virally with red fluorescent protein (RFP; pDsRed2-N1, Clontech, Palo Alto, CA, USA) and human telomerase reverse transcriptase (pGRN145, American Type Culture Collection, Manassas, VA, USA) [18], were cultured in minimum essential medium Alpha (α-MEM; Life Technologies, Carlsbad, CA, USA) that contained 20% fetal bovine serum (FBS; HyClone, Logan, UT, USA), 30 μg/mL hygromycin B, and 200 μg/mL geneticin (Life Technologies). The HUVECs were cultivated in Medium 199 (Life Technologies) that was supplemented with 10% FBS and 1% penicillin–streptomycin (Life Technologies). Cells were grown at 37 °C in a humidified incubator with 5% (v/v) CO_2.

2.2. Construction and characterization of 3D HUVEC/cbMSC aggregates

The 3D aggregates of HUVECs/cbMSCs were constructed in α-MEM that contained 20% FBS and 1% penicillin–streptomycin, using a thermo-responsive MC hydrogel system that was created in 96-well plates [19,20]. Briefly, equal amounts of HUVECs and cbMSCs were suspended in a culture medium, which was then added to each well that contained the MC hydrogel system (5×10^3 cells of each type per well), and then cultivated for 24 h with orbital shaking at 85 rpm (Fig. 1). The cell aggregates thus formed were collected and fixed in 4% paraformaldehyde (Sigma–Aldrich, St. Louis, MO, USA), before being cryosectioned at 10 μm thickness and stained with antibodies against von Willebrand factor (vWF; Dako, Glostrup, Denmark), fibronectin or hypoxia-inducible factor (HIF)-1α (Abcam, Cambridge, MA, USA); they were then incubated with Alexa Fluor 488-conjugated secondary antibodies (Life Technologies), mounted with 4,6-diamidino-2-phenylindole (DAPI; Vector Laboratories, Burlingame, CA, USA), and visualized using confocal laser scanning microscopy (CLSM; Carl Zeiss, Jena GmbH, Germany). Cell viability was investigated using a live/dead staining kit (Life Technologies), in which the hydrolysis of calcein-AM in live cells generated green fluorescence, while the ethidium homodimer produced red fluorescence in dead cells.

2.3. Tube formation assay

The grown cell aggregates were transferred onto growth factor-reduced Matrigel (BD Biosciences, San Jose, CA, USA)-coated μ-Dish (ibidi, Munich, Germany). On days 1, 4, 7, 10, and 14, the immunofluorescence staining of the tubular structures that were grown on Matrigel was carried out with anti-vWF and anti-$\alpha_v\beta_3$ integrin antibodies, visualized by fluorophore-conjugated secondary antibodies (Life Technologies), counterstained with DAPI, and observed by CLSM. Concomitantly, the culture media were collected and analyzed by the Procarta Plex Cytokine assay ($n = 6$; Affymetrix, Santa Clara, CA, USA).

2.4. Animal study

All animal experiments in this study conformed to the "Guide for the Care and Use of Laboratory Animals" of the Institute of Laboratory Animal Resources, National Research Council, published by the National Academy Press in 1996. The Institutional Animal Care and Use Committee of Veterans General Hospital (Taichung, Taiwan) reviewed and approved all animal protocols. Lewis rats that weighed 250–300 g underwent permanent ligation of the left coronary artery to induce acute MI [21–23]. Animals that fulfilled the echocardiographic inclusion criterion by exhibiting left ventricular fractional shortening <35% were used in the subsequent experiments. These animals were intramyocardially injected with saline, dissociated HUVECs/cbMSCs (1×10^6 cells each type per rat), or 3D HUVEC/cbMSC aggregates (200 cell aggregates per rat,

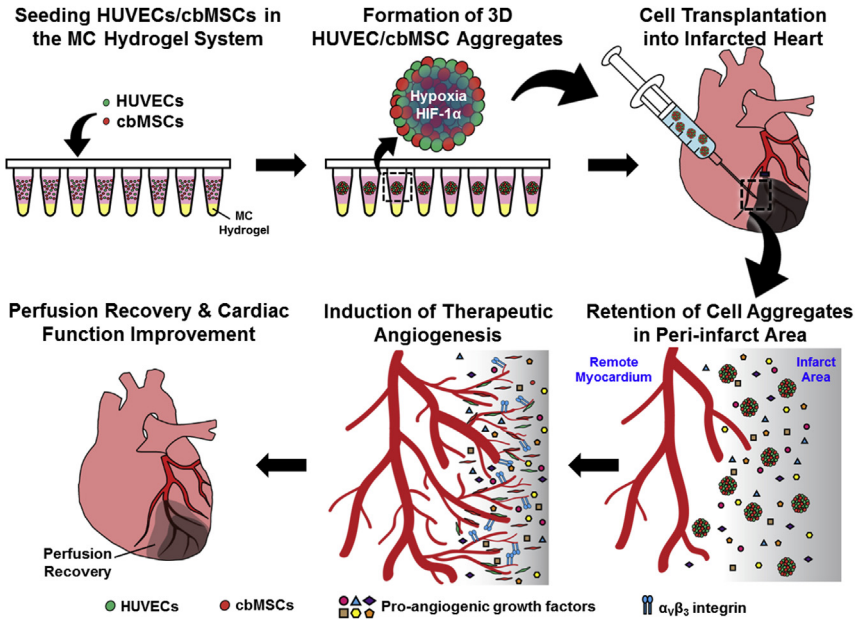

Fig. 1. Schematic illustrations of the construction of 3D aggregates of HUVECs/cbMSCs in a methylcellulose (MC) hydrogel system and use of these cell aggregates to treat myocardial infarction in rats. 3D cell aggregates were intramyocardially transplanted into peri-infarct areas. Engrafted cells induced significant therapeutic angiogenesis by direct formation of neovasculatures or by indirect paracrine secretion of pro-angiogenic factors, enhancing myocardial blood perfusion and improving post-infarcted cardiac function.

equivalent to 1×10^6 cells each type) in the peri-infarct zones. Immunosuppression was realized by intramuscularly administering cyclosporine A (Novartis, Rueil-Malmaison, France) at a dose of 10 mg/kg/day from three days before transplantation until the animals were euthanized.

2.5. SPECT and PET imaging

The myocardial perfusion of the animals under light sedation (2% isoflurane in oxygen) was observed noninvasively using high-sensitivity SPECT. SPECT imaging was conducted using a NanoSPECT/CT scanner (Bioscan, Washington DC, USA) three days following MI induction (as the baseline) and four weeks following cell treatment ($n = 5$ for each test group). One hour before the acquisition of SPECT images, animals were intravenously administered ^{99m}Tc-sestamibi (74 MBq); images were acquired for 20 min.

The post-infarcted angiogenesis of each animal was studied by PET (Siemens Medical Solutions, Knoxville, TN, USA) on day five after cell treatment, at which time the myocardial angiogenesis peaked (data not shown). In this experiment, gallium-68 (^{68}Ga), a radioisotope, was immobilized on an arginine-glycine-aspartic acid (RGD) peptide as a tracer for PET imaging. Test animals were intravenously injected with ^{68}Ga-RGD (37 MBq) at 45 min before the PET image acquisition began ($n = 5$ for each group); the PET images were acquired for 30 min.

The acquired SPECT and PET images were evaluated using image analysis software (PMOD Technologies, Zurich, Switzerland). The PMOD Cardiac Modeling Tool was employed to produce the myocardial contours. To quantify the size of the perfusion defect, the activity of the tracer was normalized to its maximum value and shown as a 2D polar map with 17 segments, or it was reconstructed three-dimensionally. The area of the perfusion defect was defined as the fraction of the polar-map elements whose tracer-uptakes were diminished by more than 50% of their maximum uptakes [24]. The percentage perfusion recovery was the reduction in the size of the perfusion defect divided by the original size of the defect $\times$ 100%. In the PET images, the mean radioactivity was expressed as a percentage of the injected dose per gram (%ID/g).

2.6. Echocardiography

Echocardiography was performed to assess the global cardiac function of test animals at the baseline and at four weeks following cell treatment ($n = 6$ for each studied group). An ultrasound system (Vivid E9, GE Healthcare, Wauwatosa, WI, USA), equipped with a 4–12 MHz phased-array transducer, was used to capture 2D images and M-mode tracings in standard parasternal short-axis views. The LV end systolic dimension (LVESD) and end diastolic dimension (LVEDD) were determined using M-mode tracings. The LV end diastolic volume (LVEDV) and end systolic volume (LVESV) were then calculated by applying the Teichholz formula [25], and the LV ejection fraction (LVEF) was estimated as LVEF (%) = [(LVEDV − LVESV)/LVEDV] × 100% [25]. To compare the effects of treatment, changes in LVEF (ΔLVEF) were also calculated as (LVEF after four weeks)−(LVEF at baseline).

To evaluate regional cardiac function, the LV was divided into six segments (anterior, anteroseptal, inferoseptal, inferior, inferolateral, and anterolateral); their strains, which are changes in length divided by the original lengths [26], in the circumferential and radial directions were calculated using a speckle-tracking algorithm (EchoPAC, GE Healthcare). The sum of the areas of the anterior and anterolateral segments was defined as the infarct area; the sum of the areas of the anteroseptal and inferolateral segments was described as the peri-infarct area and the sum of the areas of the inferoseptal and inferior segments was the remote area [25]. The strain associated with each area was calculated as the average of the two segments and expressed as a percentage (%); the change of strain between the baseline and four weeks after treatment was also estimated.

2.7. Histological analyses

Four weeks after cell transplantation, samples of LV myocardium were harvested from test animals, fixed in 10% phosphate-

buffered formalin, embedded in paraffin, and then sectioned for subsequent histological analyses. Masson's trichrome staining was performed to evaluate ventricular morphology and myocardial fibrosis. The morphometric parameters (the infarct size, infarct wall thickness, LV cavity area, and total LV area) were evaluated using the Image-Pro® Plus software (Media Cybernetics, Silver Spring, MD, USA) [27]. The LV expansion index, which is an index of LV dilation, was obtained as (area of LV cavity/total LV area) × (non-infarcted wall thickness/infarcted wall thickness) [27].

Capillary and arteriole densities were separately obtained by immunohistochemical staining with antibodies against vWF and smooth muscle actin (SMA; Dako), respectively. The numbers of capillaries and arterioles per unit area (mm^2) were blindly calculated using Image-Pro® Plus software. For immunofluorescence staining, tissue samples were incubated with primary antibodies against vWF, SMA, or RFP. Fluorescent signals were amplified with suitable Alexa Fluor-conjugated secondary antibodies. The stained sections were counterstained with DAPI and then examined by CLSM.

2.8. Statistical analysis

Data are expressed as mean ± standard deviation. Statistical analyses were performed in SPSS (Chicago, IL, USA). To make statistical comparison between any two groups, the one-tailed Student *t* test was employed; to make the comparisons among three or more groups, one-way analysis of variation (ANOVA) was followed by the Bonferroni *post hoc* test. The Pearson's correlation coefficient was calculated to assess the correlation between percentage perfusion recovery and change in cardiac function/myocardial strains. Differences are considered significant at $P < 0.05$.

3. Results and discussion

Cell-based therapeutic angiogenesis to alleviate post-infarcted LV remodeling and dysfunction has been shown to be safe and clinically applicable [1]. This work demonstrates that the exogenous engraftment of 3D aggregates of HUVECs/cbMSCs in rats with MI promotes robust angiogenesis in the ischemic myocardium, considerably improving blood perfusion and regional LV mechanics, and restoring post-infarcted global cardiac function. Multimodality noninvasive imaging with SPECT, PET and echocardiography was performed to elucidate cell-mediated angiogenesis and its correlation with therapeutic benefits in attenuating adverse cardiac remodeling and preserving ventricular function.

3.1. Construction of 3D HUVEC/cbMSC aggregates and their characteristics

To construct 3D cell aggregates, premixed cell suspensions that contained HUVECs and cbMSCs were co-cultured in a 96-well MC-hydrogel system. The hydrated surface of the MC hydrogel, being hydrophilic and electrically neutral, prevented both the adsorption of proteins and the attachment of cells, promoting the assembly of the seeded cells [28]. Within 24 h, a cell aggregate with uniformly mixed HUVECs (cyan) and cbMSCs (red) formed in each well (Fig. 2). The constructed cell aggregates were then harvested using a multichannel pipette. Since no proteolytic enzymes were employed in harvesting the cell aggregates, the cells in the aggregates adhered to each other by bonding to ECM molecules, such as fibronectin, maximizing the cell–cell and cell–ECM communications that are crucial to the survival and retention of cells following transplantation [3]. Each cell aggregate was spherical with a radius of around 150 μm.

The results of the live/dead staining reveal that most cells in the aggregates remained viable, as evidence by the prevalent green fluorescence from the live cells. However, hypoxia was present in the inner cores of the dense cellular structures, as indicated by the accumulation of HIF-1α. HIF-1α is a master regulator that can coordinate the induction of multiple angiogenic and survival factors [29]. The capacity of cell aggregates to secrete angiogenic growth factors and induce neovascularization can be greatly enhanced by effectively switching on HIF-1α-regulated pro-angiogenic pathways.

3.2. Angiogenic potency of 3D HUVEC/cbMSC aggregates

The angiogenic potency of 3D aggregates of HUVECs/cbMSCs was examined using the *in vitro* Matrigel tube-formation assay that closely models the *in vivo* processes of sprouting angiogenesis [30]. The grown tubular networks were fixed and immunostained at predetermined times to identify $\alpha_v\beta_3$ integrin. The $\alpha_v\beta_3$ integrin, which mediates EC migration, proliferation, and survival, is the critical cell-surface receptor and adhesion molecule that is expressed in the formation of blood vessels [14,15]. The control was a co-culture of dissociated HUVECs and cbMSCs on Matrigel in a conventional 2D format.

On the first day after co-culture, the dissociated cells, together with $\alpha_v\beta_3$ integrin, formed tubular networks, but these tubular-like vessels were unstable and prone to regression over time (Fig. 3a). On day 14, hardly any $\alpha_v\beta_3$ integrin was detectable in the residual tubular structures. In 2D monolayer cultures, only the lateral region of the cell was in contact with the neighboring cells, establishing the cell polarization that may have been responsible for the reduction of the intracellular signaling and influenced the fate of the phenotype, including its maturation and the stability of the formed tubes [7].

Culturing 3D aggregates of HUVECs/cbMSCs on Matrigel formed widespread tubular networks that matured and stabilized with time. An increase in the amount of $\alpha_v\beta_3$ integrin was clearly observed in the formed tubular structures (Fig. 3a and b), revealing that the angiogenic potency of 3D cell aggregates exceeded that of their dissociated counterparts. Unlike in a conventional 2D culture, intensive direct cell–cell and cell–ECM interactions in a 3D phenotype can establish a communication network that mimics the specificity of real tissues, in which the cells are associated with various molecules and surrounded by neighboring cells. Accordingly, 3D cell aggregates have the potential to develop mature and stable tubular vessels.

In addition to contributing directly to the formation of neovasculatures, MSCs can promote angiogenesis *via* the indirect paracrine secretions of several pro-angiogenic, pro-survival, and mobilizing factors in the development of tubular networks. As pro-angiogenic factors, vascular endothelial growth factor A (VEGF-A) and fibroblast growth factor 2 (FGF-2) have major roles in vasculature development [31,32], and placenta growth factor (PlGF) amplifies the angiogenic activity of VEGF and stimulates arteriogenesis [33]. Hepatocyte growth factor (HGF) and epidermal growth factor (EGF) are powerful pro-survival factors and potent mitogens for vascular ECs [31,34], whereas stem cell factor (SCF), which is a mobilizing factor, contributes to the homing of bone-marrow progenitor cells [35].

The concentrations of the paracrine growth factors that were present in the culture media following the above tube-formation assay were analyzed. According to Fig. 3c, the concentrations of all investigated paracrine growth factors increased significantly over time in the media that were cultured with dissociated cells or 3D cell aggregates; however, the increase in the latter group was greater than in the former group ($P < 0.05$). These experimental data clearly demonstrate that the 3D aggregates of HUVECs/cbMSCs have great potential in promoting angiogenesis *in vitro via* both direct and

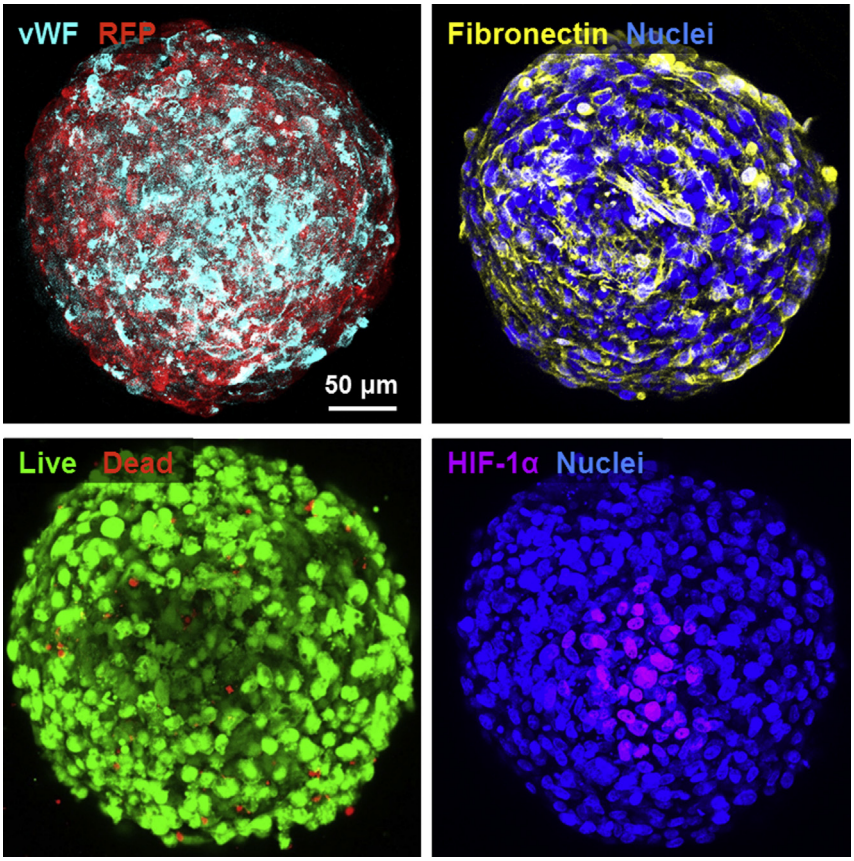

Fig. 2. Characteristics of a constructed HUVEC/cbMSC aggregate. vWF-positive HUVECs (cyan color) and RFP-expressing cbMSCs (red color) were thoroughly mixed within the cell aggregate. ECM molecules such as fibronectin were preserved in the cell aggregate. Most cells in the aggregate remained viable, as revealed by strong green fluorescence in live cells; however, hypoxia (HIF-1α) developed in the core of the cell aggregate. (For interpretation of the references to colour in this figure legend, the reader is referred to the web version of this article.)

indirect mechanisms over that achieved using their dissociated counterparts. The cell–cell contacts and cell–ECM interactions, which are crucial to the formation and stabilization of tubular networks for cells grown on Matrigel [7], are maximized for the cells that reside within the 3D cell aggregates. Additionally, hypoxia that are present in the inner cores of cell aggregates can activate the expression of numerous hypoxia-responsive angiogenic factors, promoting the formation of robust tubular structures [13].

3.3. Noninvasive molecular imaging of myocardial angiogenesis and perfusion recovery

Therapeutic angiogenesis, which increases vascular density and promotes collateral development, occurs before any significant recovery in blood perfusion and improvement in global/regional ventricular function. To investigate further their *in vivo* myocardial angiogenesis and perfusion recovery, the cell aggregates were intramyocardially engrafted into the peri-infarct areas of rats with MI and then examined noninvasively by SPECT and PET molecular imaging. ^{99m}Tc-sestamibi is a radiopharmaceutical agent that is commonly utilized in SPECT imaging to detect cardiac perfusion, while ^{68}Ga-RGD, which has a strong affinity for the angiogenic marker $\alpha_v\beta_3$ integrin, is employed as a PET imaging agent to locate and quantify myocardial angiogenesis. The areas in the images that very little or no ^{99m}Tc-sestamibi (or ^{68}Ga-RGD) could reach are the perfusion defect zones (or regions with no significant angiogenesis). The control groups received saline or dissociated cells.

SPECT and PET images of the LV myocardium on day three after the induction of MI (baseline) and at pre-determined intervals following cell transplantation were volumetrically sampled and then reconstructed as a 2D polar map or a 3D video (Fig. 4a and Supplementary Video 1); the size of each perfusion defect and percentage perfusion recovery were analyzed using image analysis software (Fig. 4b). At the baseline, the investigated groups exhibited no statistically significant variation in perfusion defect size ($P > 0.05$), suggesting that the degrees of impairment of myocardial perfusion in all test rats following their MI induction were comparable. Soon after cell engraftment (day five), the hearts that received 3D cell aggregates took up more ^{68}Ga-RGD than did those that received saline or dissociated cells ($P < 0.05$), indicating robust angiogenesis. Four weeks later, the cell-aggregate-treated hearts exhibited a significant recovery in blood perfusion (49.1 ± 7.9% recovery), indicative a pronounced therapeutic effect, relative to the hearts that received dissociated cells (21.2 ± 8.2% recovery) or saline (22.5 ± 7.4% deterioration; Fig. 4a and b). These findings suggest that regional angiogenesis was considerably promoted in the early stage after exogenous engraftment of 3D HUVEC/cbMSC aggregates, resulting in the restoration in myocardial perfusion and reduction in defect size.

Supplementary video related to this article can be found at http://dx.doi.org/10.1016/j.biomaterials.2015.09.009.

3.4. Noninvasive assessment of global/regional cardiac function by echocardiography

In addition to molecular imaging, echocardiography was used to

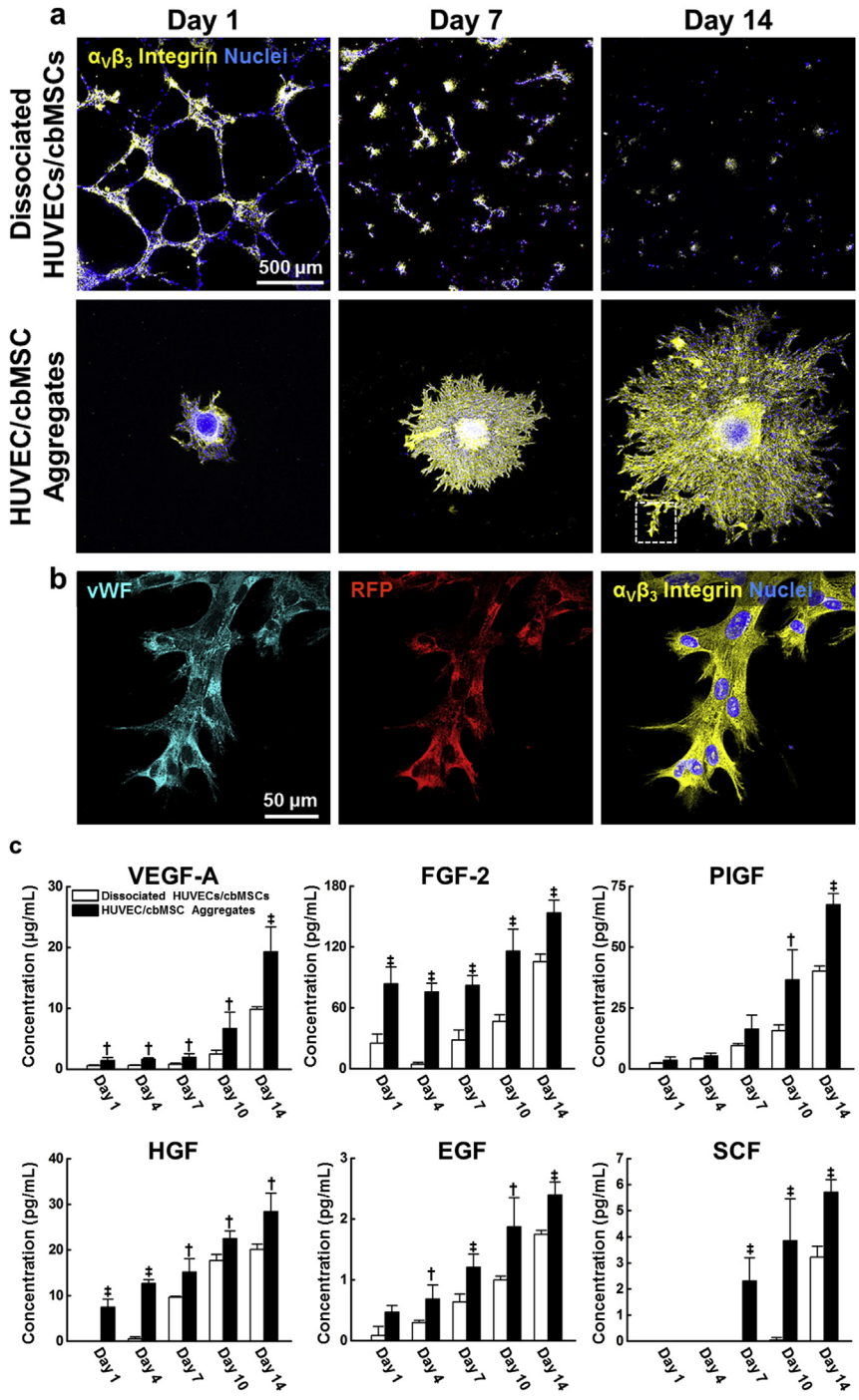

Fig. 3. Angiogenic potency of 3D HUVEC/cbMSC aggregates on Matrigel. (a) Immunofluorescence images of tubular networks with angiogenic marker $\alpha_v\beta_3$ integrin formed by dissociated cells or cell aggregates. (b) Magnified images of grown tubular structures that are indicated by dashed box in (a). (c) Temporal profiles of paracrine secretions of numerous pro-angiogenic, pro-survival, and mobilizing factors during development of tubular networks (n = 6). $^{\dagger}P < 0.05$ *vs.* dissociated-cell group; $^{\ddagger}P < 0.001$ *vs.* dissociated-cell group.

assess noninvasively the global and regional cardiac function in each test animal. The M-mode echocardiograms that were obtained at four weeks after cell transplantation (Fig. 5a) demonstrate that the dilation of LV was more attenuated in the hearts that were treated with HUVEC/cbMSC aggregates than in those that received saline or dissociated HUVECs/cbMSCs. Moreover, the improved global cardiac function (a higher LVEF in week four) and the beneficial effect of treatment (a positive ΔLVEF over time) of the hearts in response to an engraftment of cell aggregates were greater than in the control hearts ($P < 0.05$, Fig. 5b).

Regional LV mechanics (including the circumferential and radial strains that represent myocardial shortening and thickening, respectively) within the infarct, peri-infarct, and remote segments, were further analyzed using a speckle tracking algorithm [25]. 2D strain analysis more directly yields LV contractility than do conventional measurements of parameters of ventricular function, such as LVEF [36]. Values of myocardial strains can be either positive, corresponding to lengthening, or negative, reflecting

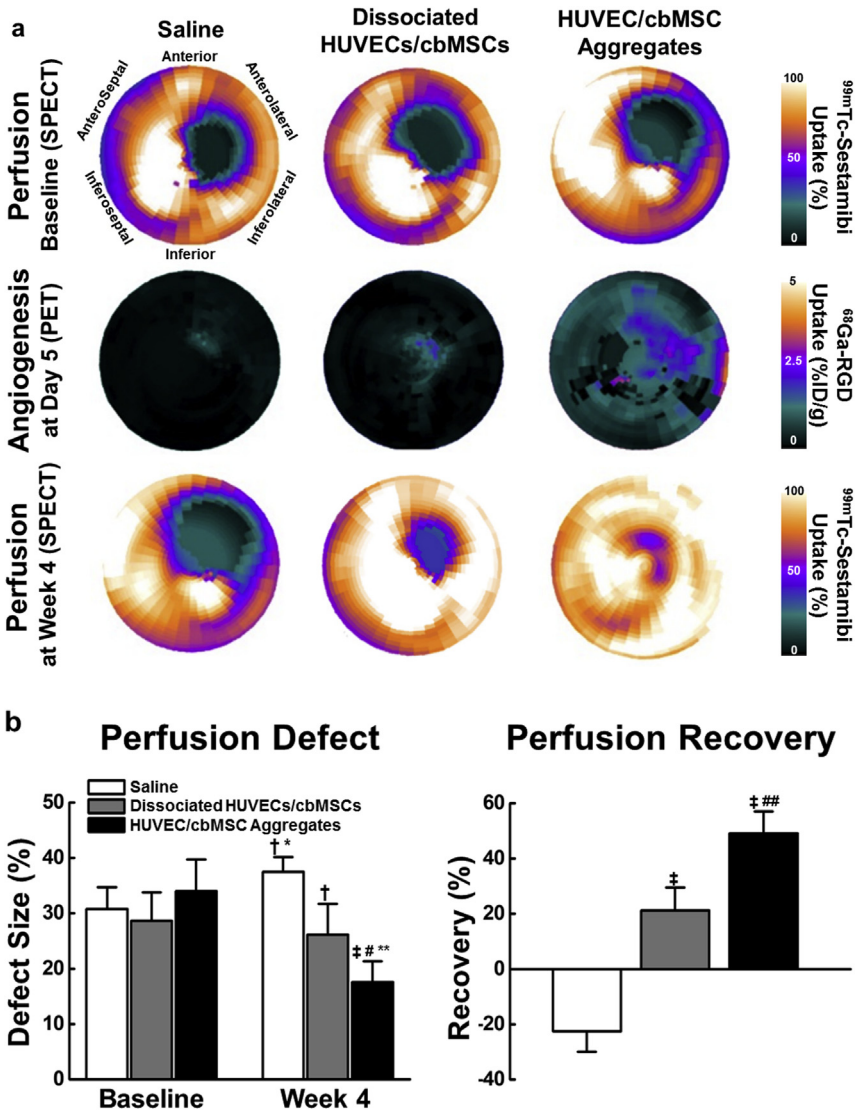

Fig. 4. Multimodality noninvasive imaging by SPECT and PET, showing myocardial perfusion and angiogenesis, respectively. (a) SPECT and PET images in polar-map format, showing perfusion defects and angiogenesis of infarcted hearts that were treated with saline, dissociated cells, or cell aggregates. (b) Quantitative results concerning size of perfusion defect and percentage perfusion recovery (n = 5). $^{\dagger}P < 0.05$ *vs.* saline group; $^{\ddagger}P < 0.001$ *vs.* saline group; $^{\#}P < 0.05$ *vs.* dissociated-cell group; $^{\#\#}P < 0.001$ *vs.* dissociated-cell group; $^{*}P < 0.05$ *vs.* same group at baseline; $^{**}P < 0.001$ *vs.* same group at baseline.

shortening. Normal values of circumferential strain are negative, whereas those of radial strain are positive. Conventionally, an LV segment that exhibits normal contractility is colored red, while that with reduced contractility is colored blue, and these colors are used in conventional 2D images.

Fig. 5c and Supplementary Videos 2 and 3 provide representative 2D strain images and their corresponding strain–time curves along the circumferential and radial directions for all investigated groups. The strain–time curves were color-coded in a manner that indicated the myocardial segments, as depicted in the figure, and their peak strain values were identified and presented in Fig. 5d. The obtained strain images reveal that the hearts that received HUVEC/cbMSC aggregates had better contractility than the control hearts. Additionally, the peak strain values suggest that the engraftment of cell aggregates significantly improved the circumferential and radial strains in the peri-infarct and infarcted zones over those in the control hearts ($P < 0.05$), suggesting an enhancement of regional wall motion.

Supplementary video related to this article can be found at http://dx.doi.org/10.1016/j.biomaterials.2015.09.009.

To elucidate the mechanisms of the functional changes in the infarcted hearts that are caused by treatment, the correlations between the recovery of myocardial perfusion and the change in LVEF (or the increase in myocardial contractility) were calculated. According to Fig. 5e, a significant correlation existed between recovery in LV perfusion and change in LVEF, suggesting that a reduction in the infarct size improved LV function. Additionally, enhanced blood perfusion in the infarcted area was correlated with improved regional circumferential and radial strains. These observations are attributable to the fact that hearts that received cell aggregates exhibited a stronger angiogenic response and a smaller perfusion defect than the control hearts that received saline or dissociated cells (Fig. 4), so their regional myocardial contractility was preserved (Fig. 5c) and their global heart function was better (Fig. 5a).

3.5. Histological analyses

The above therapeutic benefits, observed using multimodality

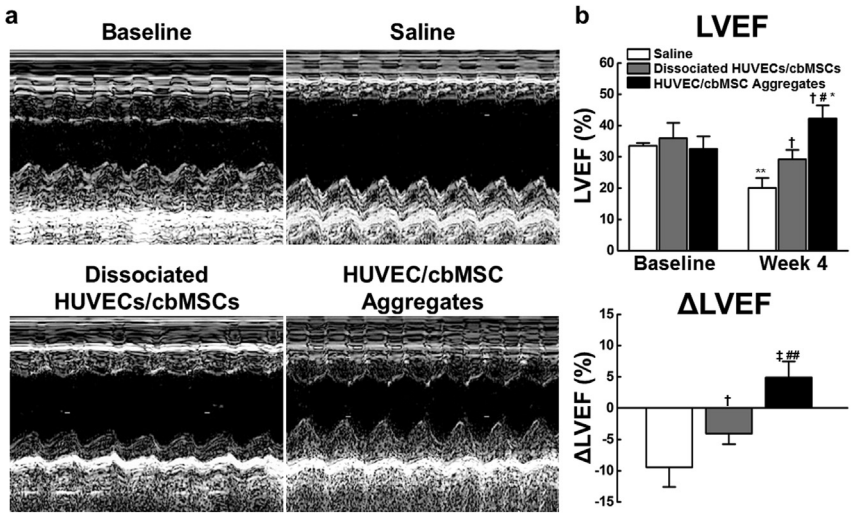

Fig. 5. Noninvasive echocardiographic assessment of global/regional cardiac function. (a) Representative M-mode echocardiograms and (b) derived left ventricular ejection fraction (LVEF) and changes in LVEF (ΔLVEF) (n = 6). (c) Circumferential and radial strain images and corresponding strain–time curves for infarct (anterior and anterolateral segments), peri-infarct (anteroseptal and inferolateral segments) and remote (inferoseptal and inferior segments) regions and (d) corresponding peak strain values. (e) Correlations of recovery in myocardial perfusion with change in LVEF (ΔLVEF) and change in myocardial contractility (Δcircumferential strain orΔradial strain) (n = 16). $^{\dagger}P < 0.05$ *vs.* saline group; $^{\ddagger}P < 0.001$ *vs.* saline group; $^{\#}P < 0.05$ *vs.* dissociated-cell group; $^{\#\#}P < 0.001$ *vs.* dissociated-cell group; $^{*}P < 0.05$ *vs.* same group at baseline; $^{**}P < 0.001$ *vs.* same group at baseline.

noninvasive image techniques, were confirmed histologically. At four weeks after cell transplantation, the animals were euthanized, and their hearts were explanted and processed for pathological examination. As shown in Fig. 6, the Masson's trichrome-stained sections of the hearts that had been treated with saline exhibited severe transmural fibrosis, infarct wall thinning, and ventricular dilation. The cell-treated hearts exhibited a smaller scar area, attenuated anterior wall thinning, and limited LV cavity enlargement. Based on the morphometric quantification, the protective effect was more pronounced in the cell-aggregate-treated hearts, which had smaller infarcts, thicker infracted walls, and less LV dilation than the hearts that had received dissociated cells ($P < 0.05$). These results reveal that the engraftment of cell aggregates in infarcted hearts effectively attenuated their adverse ventricular remodeling, helping to maintain post-infarcted LV function.

In an attempt to explore the mechanism of the observed therapeutic effects of cell transplantation, immunohistological staining for the angiogenic marker $\alpha_v\beta_3$ integrin was conducted on tissue samples that were obtained five days after cell engraftment. According to Fig. 7a, significant expression of $\alpha_v\beta_3$ integrin was

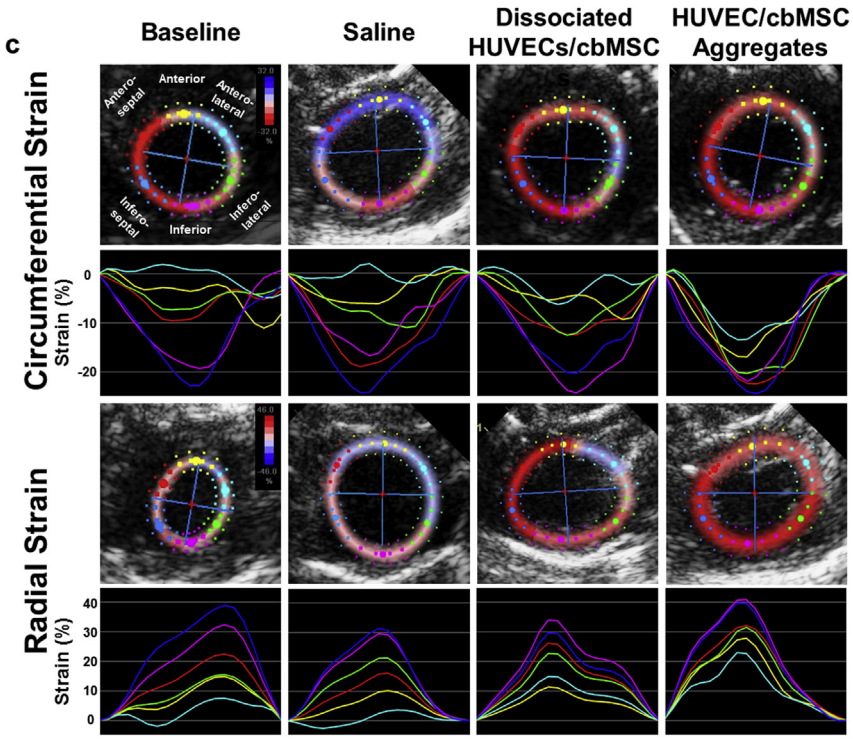

Fig. 5. (*continued*).

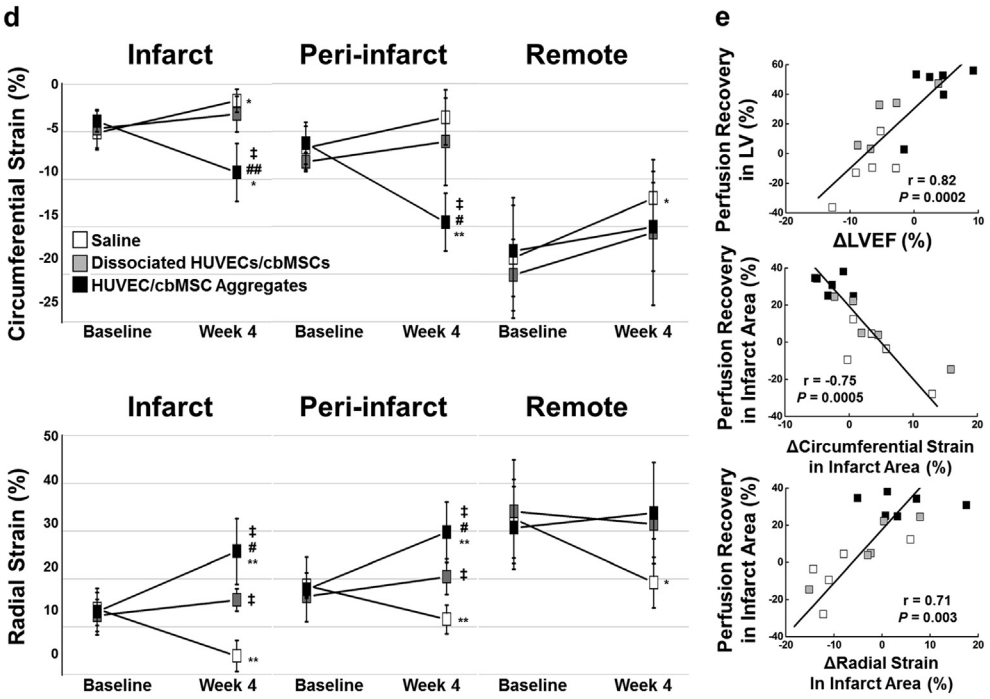

Fig. 5. (*continued*).

detectable in the cell-aggregate-treated hearts, while only a few $\alpha_v\beta_3$ integrin-positive cells were identified in the hearts that had received dissociated cells or saline ($P < 0.05$).

The capillary and arteriole densities (as obtained by staining with antibodies against vWF and SMA, respectively) in infarcted hearts that were obtained at week four were also examined. According to Fig. 7b, both the infarct and the peri-infarct zones in the hearts receiving cell aggregates contained significantly more capillaries and arterioles than did those in the hearts that received saline or dissociated cells ($P < 0.05$). Comparing these histological findings with the noninvasive imaging data in Figs. 4 and 5 reveals that exogenous engraftment of HUVEC/cbMSC aggregates into the peri-infarct zones significantly promoted the formation of functional neovasculatures, augmenting regional blood perfusion and restoring the post-infarcted ventricular function.

To determine the cellular fate and function of the engrafted aggregates of HUVECs/cbMSCs, test samples were immunohistologically stained to identify the exogenously transplanted cells. As presented in Fig. 8, the transplanted HUVECs and cbMSCs were incorporated into the vascular structures. Furthermore, the RFP-transfected cbMSCs expressed SMA, suggesting smooth muscle differentiation. These experimental results show that the

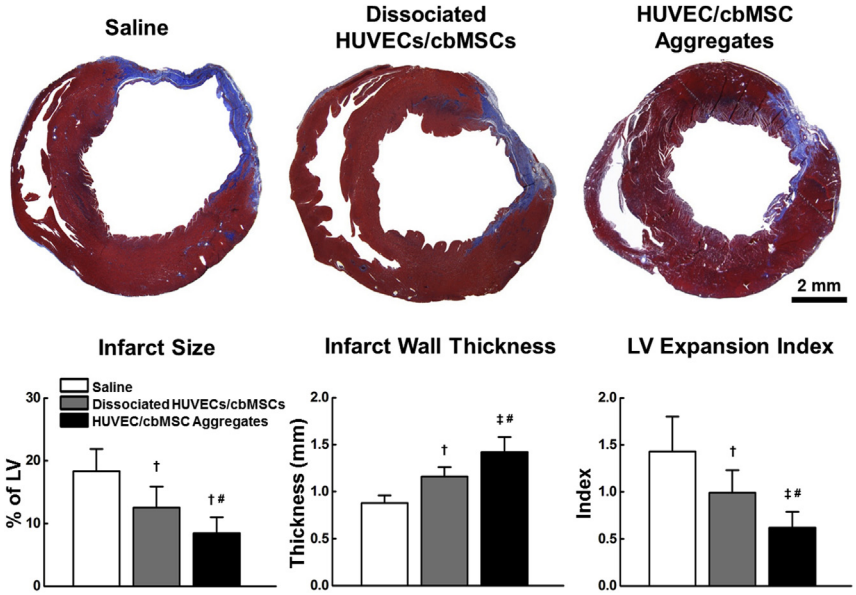

Fig. 6. Morphometric analyses of heart sections upon retrieval. Sections were Masson's trichorme-stained for histological assessment of infarct size, infarct wall thickness, and LV expansion index (n = 6). $^{\dagger}P < 0.05$ *vs.* saline group; $^{\ddagger}P < 0.001$ *vs.* saline group; $^{\#}P < 0.05$ *vs.* dissociated-cell group.

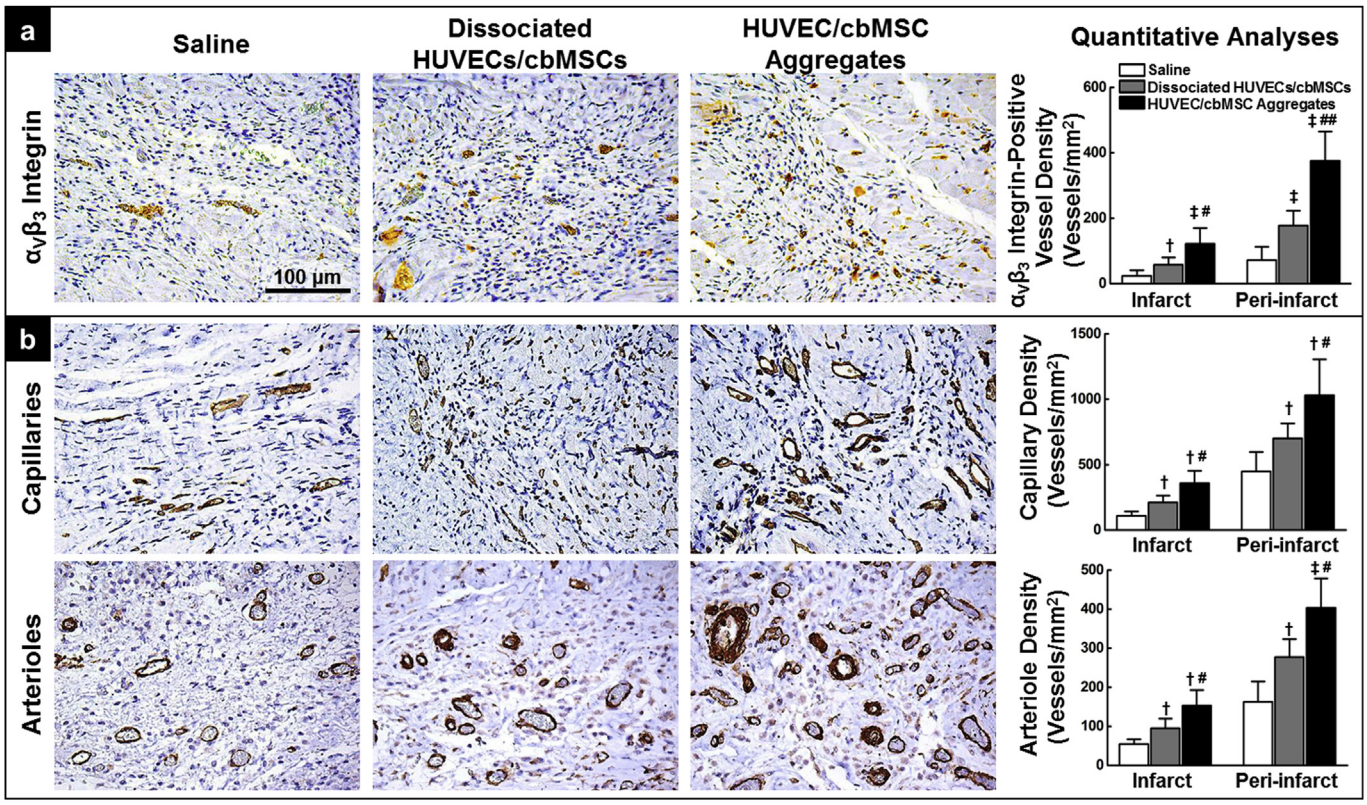

Fig. 7. Evaluation of angiogenic responses by immunohistological staining. (a) Images of angiogenic marker $\alpha_v\beta_3$ integrin in infarcted hearts retrieved on day five after cell engraftment and corresponding quantitative results (n = 6). (b) Images of vWF and SMA staining, showing densities of capillaries and arterioles in infarcted hearts retrieved four weeks after cell treatment and corresponding quantitative results (n = 6). $^{\dagger}P < 0.05$ *vs.* saline group; $^{\ddagger}P < 0.001$ *vs.* saline group; $^{\#}P < 0.05$ *vs.* dissociated-cell group; $^{\#\#}P < 0.001$ *vs.* dissociated-cell group.

transplanted HUVEC/cbMSC aggregates were directly involved in the formation of functional vessels within the ischemic myocardium, improving the post-infarcted cardiac function. Direct differentiation and indirect paracrine signaling have both been identified as the mechanisms by which MSCs stimulate angiogenesis [37].

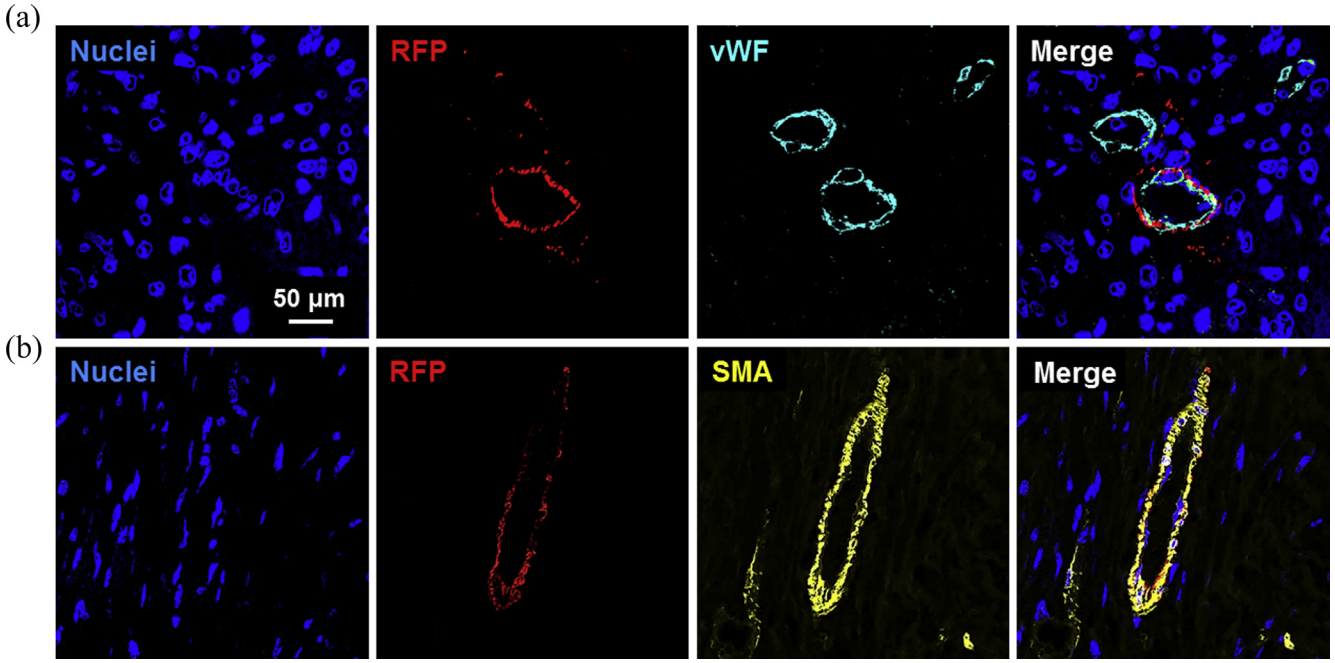

Fig. 8. *In vivo* cellular fate of engrafted cbMSCs. Immunofluorescence images of hearts four weeks after treatment with 3D HUVEC/cbMSC aggregates. Sections were stained for (a) RFP and vWF to detect luminal structures and (b) RFP and SMA to elucidate the differentiation of cbMSCs.

4. Conclusions

The present investigation reveals that the 3D aggregates of HUVECs/cbMSCs that were constructed in the study have great potential to promote angiogenesis *in vitro via* both direct and indirect mechanisms over that realized by their dissociated counterparts. Multimodality noninvasive imaging with PET, SPECT, and echocardiography enables precise characterization of the therapeutic benefits of cell engraftment in rats with MI. The *in vivo* results indicate that transplantation of 3D cell aggregates promotes cardiac repair by inducing substantial therapeutic angiogenesis, leading to recovery in blood perfusion and improvement in global/regional ventricular function. Understanding the mechanism of *in vivo* therapeutic angiogenesis induced by the cell aggregates in the study may provide foundations for advanced treatments on MI.

Acknowledgments

This work was supported by grants from the Ministry of Science and Technology (NSC 102-2320-B-075A-001-MY3 and NSC 101-2221-E-075A-001-MY3) and the National Health Research Institute (NHRI-EX103-10138EI), Taiwan. The SPECT and PET imaging studies were carried out with the help of the Center of Advanced Molecular Imaging and Translation, Chang Gung Memorial Hospital, Linkou, Taiwan.

References

[1] K. Malliaras, R.R. Smith, H. Kanazawa, K. Yee, J. Seinfeld, E. Tseliou, et al., Validation of contrast-enhanced magnetic resonance imaging to monitor regenerative efficacy after cell therapy in a porcine model of convalescent myocardial infarction, Circulation 128 (2013) 2764–2775.
[2] J.P. Cooke, D.W. Losordo, Modulating the vascular response to limb ischemia: angiogenic and cell therapies, Circ. Res. 116 (2015) 1561–1578.
[3] Z. Ye, Y. Zhou, H. Cai, W. Tan, Myocardial regeneration: roles of stem cells and hydrogels, Adv. Drug Deliv. Rev. 63 (2011) 688–697.
[4] M. Kawamura, S. Miyagawa, S. Fukushima, A. Saito, K. Miki, E. Ito, et al., Enhanced survival of transplanted human induced pluripotent stem cell-derived cardiomyocytes by the combination of cell sheets with the pedicled omental flap technique in a porcine heart, Circulation 128 (2013) S87–S94.
[5] C.C. Huang, Z.X. Liao, D.Y. Chen, C.W. Hsiao, Y. Chang, H.W. Sung, Injectable cell constructs fabricated via culture on a thermoresponsive methylcellulose hydrogel system for the treatment of ischemic diseases, Adv. Healthc. Mater. 3 (2014) 1133–1148.
[6] D.Y. Chen, H.J. Wei, W.W. Lin, K.J. Lin, C.C. Huang, C.T. Wu, et al., Intramuscular delivery of 3D aggregates of HUVECs and cbMSCs for cellular cardiomyoplasty in rats with myocardial infarction, J. Control Release 172 (2013) 419–425.
[7] D.Y. Chen, H.J. Wei, K.J. Lin, C.C. Huang, C.C. Wang, C.T. Wu, et al., Three-dimensional cell aggregates composed of HUVECs and cbMSCs for therapeutic neovascularization in a mouse model of hindlimb ischemia, Biomaterials 34 (2013) 1995–2004.
[8] W.Y. Lee, H.J. Wei, J.J. Wang, K.J. Lin, W.W. Lin, D.Y. Chen, et al., Vascularization and restoration of heart function in rat myocardial infarction using transplantation of human cbMSC/HUVEC core-shell bodies, Biomaterials 33 (2012) 2127–2136.
[9] R.K. Jain, Molecular regulation of vessel maturation, Nat. Med. 9 (2003) 685–693.
[10] M. Crisan, S. Yap, L. Casteilla, C.W. Chen, M. Corselli, T.S. Park, et al., A perivascular origin for mesenchymal stem cells in multiple human organs, Cell Stem Cell 3 (2008) 301–313.
[11] A.P. Napolitano, P. Chai, D.M. Dean, J.R. Morgan, Dynamics of the self-assembly of complex cellular aggregates on micromolded nonadhesive hydrogels, Tissue Eng. 13 (2007) 2087–2094.
[12] J. Lee, M.J. Cuddihy, N.A. Kotov, Three-dimensional cell culture matrices: state of the art, Tissue Eng. Part B Rev. 14 (2008) 61–86.
[13] C.C. Huang, D.Y. Chen, H.J. Wei, K.J. Lin, C.T. Wu, T.Y. Lee, et al., Hypoxia-induced therapeutic neovascularization in a mouse model of an ischemic limb using cell aggregates composed of HUVECs and cbMSCs, Biomaterials 34 (2013) 9441–9450.
[14] H. Hong, F. Chen, Y. Zhang, W. Cai, New radiotracers for imaging of vascular targets in angiogenesis-related diseases, Adv. Drug Deliv. Rev. 76 (2014) 2–20.
[15] L.L. Johnson, L. Schofield, T. Donahay, M. Bouchard, A. Poppas, R. Haubner, Radiolabeled arginine-glycine-aspartic acid peptides to image angiogenesis in swine model of hibernating myocardium, JACC Cardiovasc. Imaging 1 (2008) 500–510.
[16] L. Lamalice, F. Le Boeuf, J. Huot, Endothelial cell migration during angiogenesis, Circ. Res. 100 (2007) 782–794.
[17] S. De, O. Razorenova, N.P. McCabe, T. O'Toole, J. Qin, T.V. Byzova, VEGF-integrin interplay controls tumor growth and vascularization, Proc. Natl. Acad. Sci. U. S. A. 102 (2005) 7589–7594.
[18] C.J. Hung, C.L. Yao, F.C. Cheng, M.L. Wu, T.H. Wang, S.M. Hwang, Establishment of immortalized mesenchymal stromal cells with red fluorescence protein expression for in vivo transplantation and tracing in the rat model with traumatic brain injury, Cytotherapy 12 (2010) 455–465.
[19] W.Y. Lee, Y.H. Chang, Y.C. Yeh, C.H. Chen, K.M. Lin, C.C. Huang, et al., The use of injectable spherically symmetric cell aggregates self-assembled in a thermoresponsive hydrogel for enhanced cell transplantation, Biomaterials 30 (2009) 5505–5513.
[20] W.Y. Lee, H.J. Wei, W.W. Lin, Y.C. Yeh, S.M. Hwang, J.J. Wang, et al., Enhancement of cell retention and functional benefits in myocardial infarction using human amniotic-fluid stem-cell bodies enriched with endogenous ECM, Biomaterials 32 (2011) 5558–5567.
[21] W.E. Wang, D. Yang, L. Li, W. Wang, Y. Peng, C. Chen, et al., Prolyl hydroxylase domain protein 2 silencing enhances the survival and paracrine function of transplanted adipose-derived stem cells in infarcted myocardium, Circ. Res. 113 (2013) 288–300.
[22] C. Huang, X. Zhang, J.M. Ramil, S. Rikka, L. Kim, Y. Lee, et al., Juvenile exposure to anthracyclines impairs cardiac progenitor cell function and vascularization resulting in greater susceptibility to stress-induced myocardial injury in adult mice, Circulation 121 (2010) 675–683.
[23] M.A. Laflamme, K.Y. Chen, A.V. Naumova, V. Muskheli, J.A. Fugate, S.K. Dupras, et al., Cardiomyocytes derived from human embryonic stem cells in pro-survival factors enhance function of infarcted rat hearts, Nat. Biotechnol. 25 (2007) 1015–1024.
[24] M.C. Wu, D.W. Gao, R.E. Sievers, R.J. Lee, B.H. Hasegawa, M.W. Dae, Pinhole single-photon emission computed tomography for myocardial perfusion imaging of mice, J. Am. Coll. Cardiol. 42 (2003) 576–582.
[25] M. Kawamura, S. Miyagawa, K. Miki, A. Saito, S. Fukushima, T. Higuchi, et al., Feasibility, safety, and therapeutic efficacy of human induced pluripotent stem cell-derived cardiomyocyte sheets in a porcine ischemic cardiomyopathy model, Circulation 126 (2012) S29–S37.
[26] B.D. Hoit, Strain and strain rate echocardiography and coronary artery disease, Circ. Cardiovasc. Imaging 4 (2011) 179–190.
[27] X.L. Tang, G. Rokosh, S.K. Sanganalmath, F. Yuan, H. Sato, J. Mu, et al., Intracoronary administration of cardiac progenitor cells alleviates left ventricular dysfunction in rats with a 30-day-old infarction, Circulation 121 (2010) 293–305.
[28] C.C. Wang, C.H. Chen, S.M. Hwang, W.W. Lin, C.H. Huang, W.Y. Lee, et al., Spherically symmetric mesenchymal stromal cell bodies inherent with endogenous extracellular matrices for cellular cardiomyoplasty, Stem Cells 27 (2009) 724–732.
[29] G.L. Semenza, Hypoxia-inducible factors in physiology and medicine, Cell 148 (2012) 399–408.
[30] A.R. Reynolds, I.R. Hart, A.R. Watson, J.C. Welti, R.G. Silva, S.D. Robinson, et al., Stimulation of tumor growth and angiogenesis by low concentrations of RGD-mimetic integrin inhibitors, Nat. Med. 15 (2009) 392–400.
[31] E.C. Novosel, C. Kleinhans, P.J. Kluger, Vascularization is the key challenge in tissue engineering, Adv. Drug Deliv. Rev. 63 (2011) 300–311.
[32] L. Coultas, K. Chawengsaksophak, J. Rossant, Endothelial cells and VEGF in vascular development, Nature 438 (2005) 937–945.
[33] A. Luttun, M. Tjwa, L. Moons, Y. Wu, A. Angelillo-Scherrer, F. Liao, et al., Revascularization of ischemic tissues by PlGF treatment, and inhibition of tumor angiogenesis, arthritis and atherosclerosis by anti-Flt1, Nat. Med. 8 (2002) 831–840.
[34] B. Möller, C. Rasmussen, B. Lindblom, M. Olovsson, Expression of the angiogenic growth factors VEGF, FGF-2, EGF and their receptors in normal human endometrium during the menstrual cycle, Mol. Hum. Reprod. 7 (2001) 65–72.
[35] K.L. Marcelo, L.C. Goldie, K.K. Hirschi, Regulation of endothelial cell differentiation and specification, Circ. Res. 112 (2013) 1272–1287.
[36] P. Reant, L. Labrousse, S. Lafitte, P. Bordachar, X. Pillois, L. Tariosse, et al., Experimental validation of circumferential, longitudinal, and radial 2-dimensional strain during dobutamine stress echocardiography in ischemic conditions, J. Am. Coll. Cardiol. 51 (2008) 149–157.
[37] S.H. Ranganath, O. Levy, M.S. Inamdar, J.M. Karp, Harnessing the mesenchymal stem cell secretome for the treatment of cardiovascular disease, Cell Stem Cell 10 (2012) 244–258.